M. Uzielli · F. Catani · V. Tofani · N. Casagli

Risk analysis for the Ancona landslide—I: characterization of landslide kinematics

Abstract The Ancona landslide is a complex, deep-seated landslide displaying composite rotational–translational kinematisms and affecting a large urban area in the Ancona municipality on the Adriatic coast of central Italy. The landslide was reactivated with a large and destructive event on 13 December 1982 following a long period of precipitation and has remained active since. This paper focuses on the estimation of the landslide kinematics (more specifically, the horizontal and vertical components of average yearly velocity) for subsequent estimation of risk for a set of 39 buildings as presented in a companion paper. The study relies both on the processing of inclinometer and radar interferometer monitoring data through statistical procedures. Triggering factors are not investigated. Outputs from the two sets of monitoring data are compared quantitatively and qualitatively. The inherent limitations in available data are discussed. The validity of the quantitative results in the context of the risk estimation effort is discussed.

Introduction

On the night of 13th December 1982, the city of Ancona suffered a large landslide that occurred along the coast to the north of the town, in the adjacent slopes of the Montagnolo Hill (Fig. 1). The volume of the mass movement was about 180 million m³, whereas the affected surface area was 220 ha, accounting for 11 % of the total urban area of the Ancona municipality (Cardellini and Osimani 2008). No casualties were recorded during the event. Nonetheless, the landslide caused extensive damage to structures and infrastructure, such as the University Medical Faculty and the local hospital. A total of 3,661 people (1,071 families) were evacuated from the residential districts named Posatora and Borghetto. Gas and water supplies were interrupted too, and the city remained for some days without the essential gas and water services. Two hundred eighty structures (out of a total of 865) suffered non-negligible to irreparable damage or were destroyed. Thirty-one farms, 101 SMEs, 3 industries, and 42 shops were significantly damaged, and 500 people lost their jobs. The Adriatic railway and Flaminia road were shifted laterally 10 m toward the sea.

During the event, displacements started at the toe of the slope, spreading upwards. Cotecchia (2006) reported that "large horizontal displacements of up to 8 m and uplifts of up to 3 m affected the lower parts of the slope. In the upper parts of the slope area, horizontal displacements of up to 5 m and large vertical settlements (up to 2.5 m) were recorded. The effects of the landslide movements were not restricted to on-shore areas; large displacements also occurred in the seabed adjacent to the main landslide."

Considering the significance of the Ancona landslide event, local authorities were interested in assessing the possibility to consolidate and stabilize the affected area. A campaign of geological, lithological, geophysical, geomorphologic, and geotechnical

analyses, aimed at supporting a preliminary design for remediation, was initiated. Intrusive and nonintrusive investigative techniques were used to assess the geological and geotechnical characteristics of the mass involved in the 1982 landslide, the failure mechanisms and the factors that triggered the event. Local authorities concluded that a comprehensive consolidation would have entailed very large expenses and would have brought a very severe environmental and socioeconomic impact on the area. Thus, The Ancona Municipality decided to live with the landslide while striving to ensure the safety of local residents. Nonetheless, the planned remedial scheme was partially carried out, when some stabilization works were conducted between 1999 and 2003 on the eastern part of the landslide area. A more surficial drainage system was also completed; reinforced bulkheads were built, and some parts of the landslide area were reforested. In 2002, the Regione Marche assigned the Ancona Municipality the responsibility of creating an Early Warning System and an Emergency Plan for people who are still today living in the landslide area. The Early Warning System, which is currently being improved by additional instrumentation, aims to provide an integrated and continuous control at a surficial and deep level of the entire landslide area. Details are given in Cardellini and Osimani (2008).

Any decision-making process concerning human valued assets relies (implicitly or explicitly) on the concept of risk estimation and risk management. Estimated levels of risk for one or more categories of vulnerable elements are compared with acceptable/tolerable levels. When pursued in an at least partly quantitative perspective, risk management provides a more objective and rational basis for decision-making than a purely qualitative approach. The focus of this paper is on the characterization of ground displacements in a part of the landslide area from monitoring data and qualitative inferences. Statistical methods are employed to provide in a formal framework the quantitative information necessary to perform the probabilistic risk analysis as detailed in a companion paper (Uzielli et al. 2014), in which the outputs obtained herein are used for the semiquantitative estimation of risk for a set of 39 buildings located inside the landslide area. The strengths and limitations in the implemented methods and in available data—the latter both in terms of number and quality—are discussed.

Setting and features of the Ancona landslide: an overview

Historical overview

The coastal slopes in the Ancona area are known to have been unstable for centuries. Historical records document the occurrence of significant movements in the same slope in 1578, 1768, 1858, and 1919 (Bracci 1773; De Bosis 1859; Segré 1920; Crescenti 1986). Crescenti (1986) noted the great reduction in the actual number of the building on the Montagnolo slope, compared with a cadastral map of 1915, as an evidence of the historical activity of the mass movements in 1919. Several studies (Coltorti et al. 1985,

178.00 a s.l.

2200 m

Volume of landslide mass
approx. 180 million m³
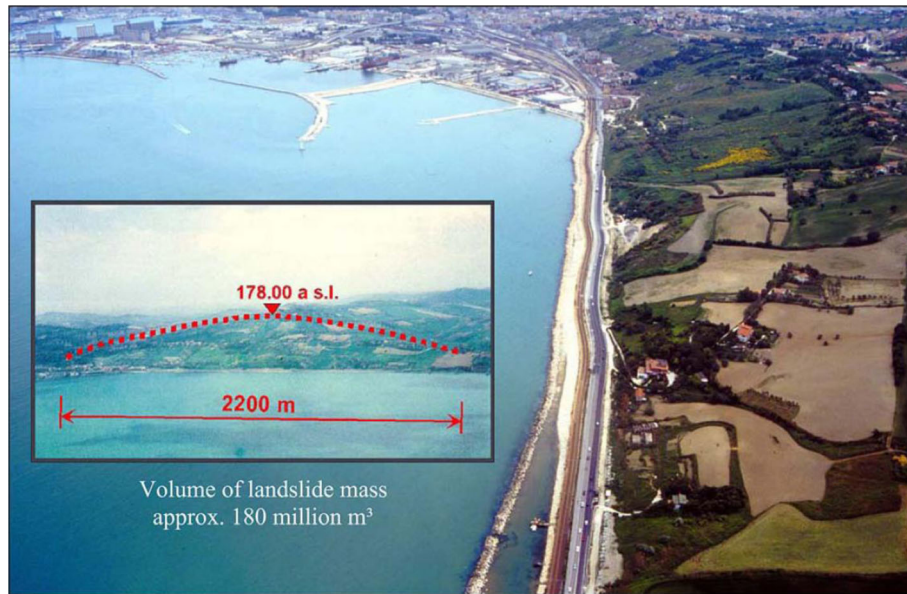
Fig. 1 Panoramic view of the Ancona landslide area (from Cotecchia 2006)

1986; Crescenti et al. 1983, 2005; Curzi and Stefanon 1986; Dramis et al. 2002) date the onset of movements on the Montagnolo slope to 5000–6000 years ago, before the Flandrian Transgression, when regional uplift brought the foredeep sediments to their present-day elevation.

Geological, tectonic, geotechnical, and hydrogeological setting

From a structural point of view, the Ancona area lies on the external margin of the Apennines, which tectonic history is directly connected to the evolution of the Adriatic foredeep (Bally et al. 1988). Figure 2 shows a geological map of the area, together with a representative geological cross section. Underlying the recent superficial cover of elluvium, colluvium, and associated landslide debris, a succession of strata belonging to the Lower, Middle, and Upper Pliocene and the Lower Pleistocene were identified. Also depicted on the geological map are traces of the Tavernelle syncline, NE–SW transcurrent faults and EW normal faults, which were formed principally as a result of several tectonic phases. The normal faults cut the Montagnolo slope (see Fig. 2) lowering the sediments toward the sea, with a maximum displacement between 50 and 150–200 m in the Lower-Middle Pliocene (Crescenti et al. 1983).

The second fault system, characterized by transverse faults with anti-Apenninic NNE–SSW orientation (Crescenti et al. 1983), was originated during the latest tectonic phase (Pleistocene to date). The landslide area is crossed by two of these faults, namely, the Borghetto and the Fornetto-Posatora faults (see Fig. 2), which dislocate the Tavarnelle syncline (Cotecchia 2006). These structures are probably still active as indicated by sources of historical earthquakes: the epicenters of the 1972–1974 earthquakes are indeed roughly aligned along these structures (Crescenti et al. 1977; Michetti and Brunamonte 2002).

The tectonic and structural setting of the Ancona area derives from several tectonic phases along the peri-Adriatic belt. Such tectonic movements, both parallel and transverse to the coastline, generated discontinuities or zones of weakness in the slope which strongly influenced the development of the failure mechanisms and

movements observed at Ancona. Crescenti et al. (1977) related the seismic activity that occurred in the area between 1972 and 1975 to movements along the existing anti-Apenninic transcurrent faults.

A considerable body of extensive studies, including geotechnical in situ and laboratory testing, were performed following the 1982 event, aiming to gain an insight into the typological characteristics of the landslide and to plan the execution and subsequent monitoring of stabilization measures (i.e., Cassinis et al. 1985; Colombo et al. 1987; Cotecchia 1994, 2000, 2001, 2006; Cotecchia et al. 1995; Cotecchia and Simeone 1996; Santaloia et al. 2004; Crescenti et al. 2005; Cardellini and Osimani 2008; Stucchi and Mazzotti 2009). The colluvial soils which are generally found at shallow depths within the slope area were found to be generally less homogeneous and plastic than the underlying Pliocene clays, which have an average clay fraction of 55 % (up to 65 %) and are classified as being of high plasticity. The Pliocene clay consistency index was found to be generally just below 1, with some samples displaying lower consistency due to their location in areas possibly disturbed by the sliding process. The compressibility of the Pliocene clays as obtained from oedometer test results was rather low ($Cc=0.30–0.35$). Direct shear and triaxial tests, for both the on-land and offshore clays indicated that the friction angles and cohesion intercept vary with increasing vertical effective stress, associated with the consolidation pressure and reducing void ratio. At medium to high pressures, the range where the on-land samples were mostly tested, the intercept cohesion reached 100 kPa and the friction angle 21°. The residual friction angles obtained from direct shear testing were around 15° for the over-land samples, decreasing to 13° for the offshore samples. Results of back-analyses conducted assuming a limit equilibrium condition for the main landslide bodies results were found to be in general agreement with the laboratory residual strengths, showing that the mobilized strength in the slope at Ancona is below the peak value. Details are given in Cotecchia (2006).

The ground water system in the area was found to be influenced by the complex structural setting including natural trenches, fractures, and discontinuities (generated both by landsliding and tectonic
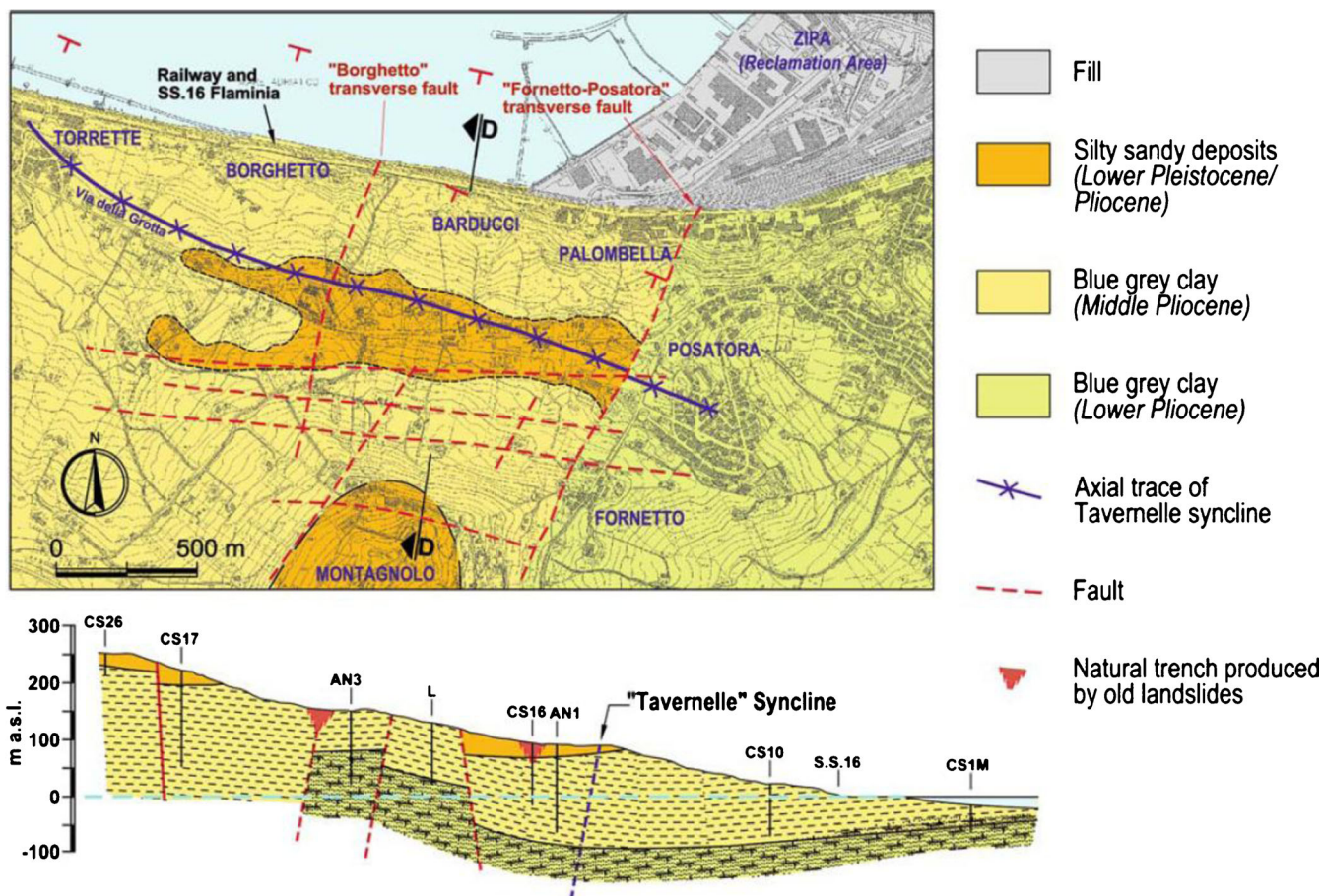
Fig. 2 Geological map and cross section of the Ancona landslide area (from Cotecchia 2006)

movements). Based on readings from piezometers installed in the area of the landslide, Cotecchia (2006) suggested the presence of a prevalent seepage domain in most of the slope, probably as a result of the high degree of fissuring of the clays and the presence of sandy interbeds, despite the presence of independent deep groundwater levels. This hypothesis was supported by the piezometric levels, which showed a decrease in depth in the uphill piezometers and an increase with depth in the piezometers near the coast. Detailed data on groundwater conditions were not available for this study.

Typological description
A vast bulk of studies (e.g., Crescenti et al. 1983, 1984, 2005; Coltorti et al. 1985, 1986; Cunietti et al. 1986; Dramis et al. 2002; Cotecchia 2006) allowed to draw a conceptual scheme of the landslide as being characterized by three main bodies with movement intermediate between rotational and translational (Cotecchia 2006): (1) a very deep and areally extensive body, defined by upper scarps at the top of the slope and extending from Palombella to Torrette, characterized by rather limited movements during 1982 event; (2) a second body, superimposed on the first, affecting the central part of the slope, which was involved in more intense deformations during the 1982 event; and (3) a third body, delimited by a lower long scarp, partly reactivated in 1982. The sliding surfaces of the three main deep landslides converge at depth into a single wide shear band with ductile behavior and low strength (Cotecchia 1994, 2006). Although

clear movements of the sea floor attributable to the 1982 event were observed only about 50 m from the coastline (Crescenti et al. 1983; Curzi and Stefanon 1986; Cotecchia 2006), the sliding surfaces of the main landslides are believed to emerge offshore, at a maximum distance from the coast line of over 250 m (Coltorti et al. 1985, 1986; Cotecchia 2006). The 1982 event saw the partial or total reactivation of the majority of the pre-existing geomorphological discontinuities, as well as the activation of several new sliding surfaces and deformation zones. A general subsidence of the central and upper part of the slope was observed, with a partial reactivation and extension of the pre-existing natural trenches, as well as a South-to-North laminar-type translational kinematism, which is most pronounced at shallower depths and has been described as being globally relatively independent from the surface morphology. Lateral rotational–translational mechanisms are also present, both in the eastern and western parts of the landslide area (in the Rupe della Palombella/Posatora and Torrette districts, respectively). Such lateral kinematisms are translationally centrifugal and rotationally oriented towards the center of the landslide body, with a West-to-East direction in the eastern part and an East-to West direction in the western part (Cotecchia 2006).

Though the 1982 event can be described as prevalently slow, rapid mudslides occurred in highly saturated colluvial soils in some areas of the landside (Cardellini and Osimani 2008). Overall, the Ancona landslide can thus be described as a deep-

seated, complex, composite landslide according to the Cruden and Varnes (1996) classification.

Presumed causes of triggering of the 1982 event

The 1982 event occurred during a rainy season characterized by six consecutive days of rain with an average intensity of 30 mm/day, corresponding to a return period of less than 10 years. Though not exceptional, the precipitation preceding the 1982 event was the highest and most unfavorable since the 1972–1973 earthquakes. Crescenti et al. (1983) opined that such a period of sustained heavy rainfall, may have caused a significantly higher net infiltration than would have been caused by a more intense but temporally limited precipitation period. Consequently, the triggering mechanism of the 1982 landslide may not have been the amount and duration of precipitation; rather, the increased permeability due to the fissuring of the clay produced by the 1972 earthquake and the probable contemporaneous reopening of the natural trenches (Crescenti et al. 1977; Michetti and Brunamonte 2002). The subvertical man-made cuts for clay quarrying also played a relevant role in accelerating slope instability processes by significantly altering slope geometry (Cotecchia 2006). The relationship between triggering factors and displacements lies beyond the scope of the study and is not addressed further.

Characterization of current slope kinematics

Risk estimation is a forward procedure which, however, must often rely on the extrapolation and future projection of data from past monitoring. This paper attempts the quantitative characterization of ongoing slope kinematics through the processing of inclinometer and interferometer measurement data and the subsequent formulation of qualitative hypotheses regarding horizontal and vertical average yearly velocities, respectively. A statistic-based approach is conceptually adequate for this purpose, as it entails the organization, analysis and processing of homogeneous data collected over time, and subsequently allows the quantitative projection of kinematic parameters for forward use in probabilistic simulation of displacement for risk estimation purposes as detailed in Uzielli et al. (2014). In pursuing a statistical approach, it is paramount to assess preliminarily the scope, presumable resolution, and character of the analysis in terms of the expected precision and accuracy of available data. Cotecchia (2006) highlighted the limitations in the quality of inclinometer measurements for the Ancona landslide, due primarily to: (a) lack of continuity in the readings over the years, resulting in a succession of different operators and equipment; (b) instrumental errors (drifting and calibration errors); and (c) operator inexperience and data processing errors. The same Author emphasized the consequent difficulty in the interpretation of the data and in the formation of a coherent kinematic model. While such limitations suggest the impossibility of pursuing a rigorous quantitative processing of monitoring data and do not advocate the use of refined statistical techniques, it is nonetheless of interest to perform a tentative quantitative analysis of measurement results as a preliminary step for risk estimation as described in Uzielli et al. (2014).

Estimation of horizontal sliding velocity

Definition of reference parameters

The estimation of horizontal ground velocity is pursued through the analysis and processing of inclinometer measurements. Data from 58

inclinometers (48 of which located inside and 10 located outside the landslide area), with at least 5 series of measurements taken between 2002 and 2008, were available. Figure 3 illustrates the locations of 51 of the 58 inclinometers (those remaining are located further away from the landslide perimeter, defined by the red line). It may be seen that inclinometer locations are not distributed uniformly throughout the area. Data obtained from inclinometer installations were used to: (a) identify the sliding surfaces and (b) investigate the sliding velocity. At any given measurement depth, the cumulative displacement ($D_{IN,c}$) is the total displacement with respect to zero-reading. The incremental displacement ($D_{IN,i}$) is the displacement with respect to previous reading.

The average daily incremental velocity (ξ_{INd}) is given by the incremental displacement between two readings divided by the number of days occurring between the two readings and is measured in millimeters per day. The average daily incremental velocity was thus projected to a yearly basis by multiplying ξ_{INd} by 365 to obtain the average yearly velocity ξ_{IN} (mm/year). This projection entails the hypothesis of temporal stationarity of sliding velocity, i.e., that there are no significant temporal trends in velocity. Such hypothesis refers to the available monitoring data collected in the period 2002–2008. In such period, no "exceptional" behavior was observed within or around the landslide perimeter, so the results obtained herein do not capture extreme scenarios such as the one which occurred in 1982. Stationarity was verified by means of Kendall's tau test, a nonparametric statistical test frequently employed in time series analysis. The test, which consists in the calculation of the "tau" test statistic and the subsequent comparison of the calculated value with thresholds related to the numerosity of the data set, provides an objective assessment of the degree of statistical independence (and, hence, of stationarity) of a data set. Kendall's tau was calculated for all data sets, resulting in the assessment of statistical independence at a 95 % confidence level. Note that the hypothesis of stationarity pertains exclusively to the data sets which were available for the study. For each inclinometer and for each pair of consecutive readings, the average velocity between consecutive readings ξ_{IN} was calculated as described above. Positive values indicate down-slope movements, whereas negative values indicate up-slope movements.

Azimuth readings were typically found to display a high variability from one reading to another (not infrequently up to 90° approximately). In accordance with previous observations, it was seen that recorded deformation azimuths within the superficial strata tend to be influenced by such factors as slope morphology and other localized features (e.g., proximity to natural trenches and maximum slope gradients). However, azimuth readings recorded in stable deeper sections were also deemed not reliable, as the general direction of movement often resulted in complete disagreement with the global movement of the main landslide body. From a quantitative perspective, in accordance with previous assessments by Cotecchia (2006), the fluctuation of azimuth readings resulted in the loss of any practical significance. Thus, azimuth readings were not considered in the analysis. The unavailability of reliable azimuth measurements, however, does not impede the characterization of slope movements for the specific purpose of risk estimation for buildings, as the landslide damaging potential for buildings can be assumed to be invariant to the direction of sliding.
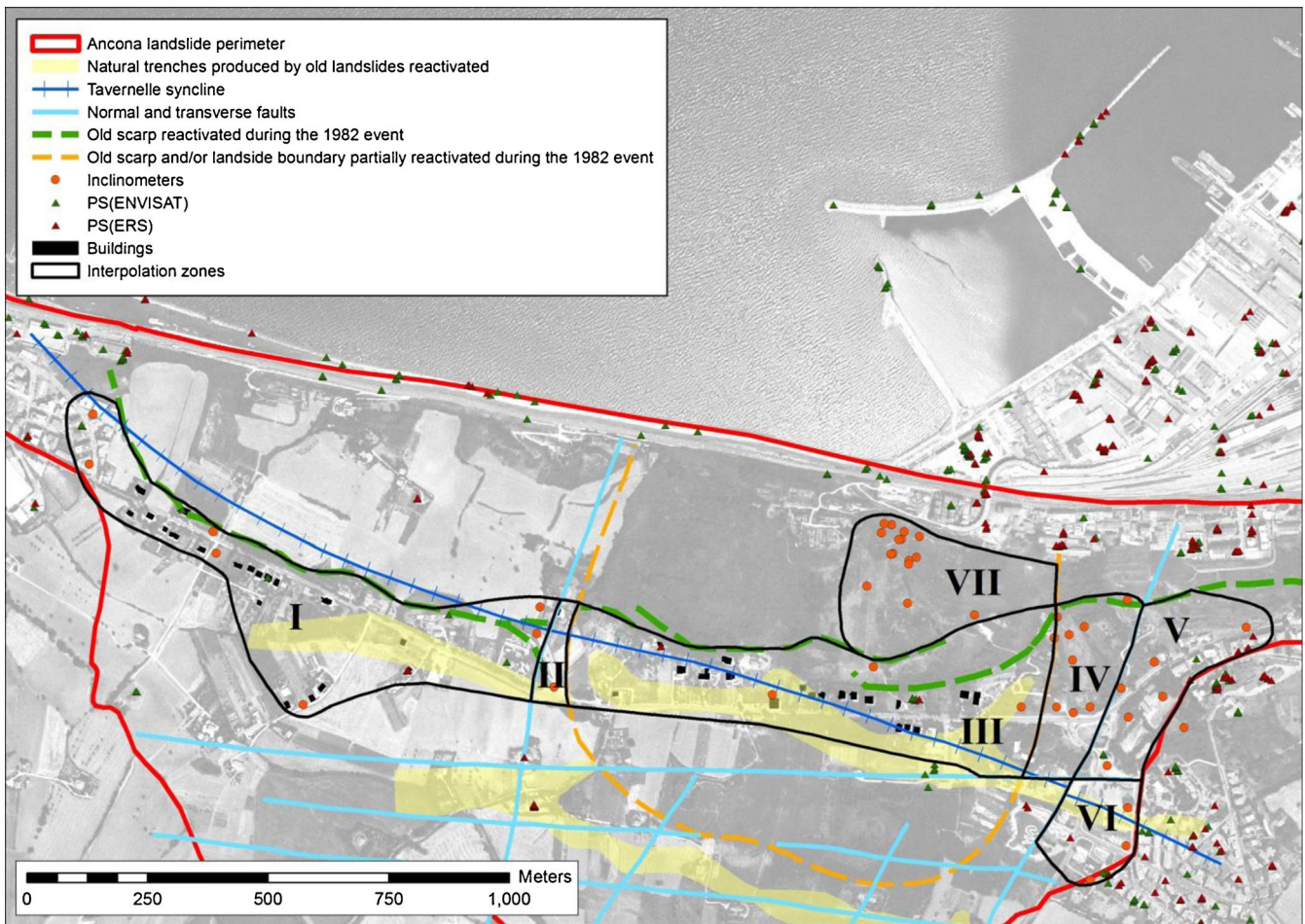
Fig. 3 Interpolation subzones, main geomorphologic features, and locations of inclinometer and SAR interferometer monitoring instrumentation

To identify relevant sliding surfaces, the differential velocity $\xi_{IN\Delta}$, given by the difference between the average velocity at one reading depth and at the reading depth immediately above, was calculated. In absence of univocal criteria, a lower differential velocity threshold $\xi_{IN\Delta t}=1$ mm year^{-1} m^{-1}, below which $\xi_{IN\Delta}$ (in absolute value) could be considered negligible for the purposes of the present analyses, was established subjectively. Instances in which $|\xi_{IN\Delta}|\geq\xi_{IN\Delta t}$ were recorded (see example in Fig. 4 for inclinometer BA04, in which data from more recent readings are shown in darker lines, and in which the dashed lines delimit the range $\pm\xi_{IN\Delta t}$). Similar plots were obtained for all inclinometers. The example shows the presence of a major sliding surface around depth 15 m bgl. Relevant differential movements at more surficial depths (from ground level to 5 m bgl approximately) are also observed. Differential sliding of significantly smaller magnitude was also recorded at other depths, but not on a continuous basis. Overall, it was observed that relevant differential sliding phenomena are quasi-continuous. These qualitative observations of the temporal distribution of differential sliding, which can be generalized for the vast majority of the inclinometers, were employed to support the hypothesis of temporal stationarity of sliding of the monitoring data available for the study, as well as the confident projection of average velocities from a trimestral to an annual reference period as discussed previously.

Statistical modeling of inclinometer data

The statistical processing of inclinometer data involved the calculation of empirical cumulative distribution functions of average yearly velocity, and the subsequent extraction of relevant sample quantiles. A set of 12 reference depths, which were deemed to be significant for the description of the kinematics of the Ancona landslide, were defined: 1, 3, 5, 10, 20, 30, 40, 50, 60, 70, 80, and 90 m bgl, (hereinafter denoted as D01, D03, D05, D10, D20, D30, D40, D50, D60, D70, D80, and D90, respectively). The empirical cumulative distribution function (ECDF) of a sample is the cumulative distribution function associated with the empirical measure of the sample itself. ECDFs of ξ_{IN} were calculated for each inclinometer and for each reference depth. For example, Fig. 5 shows the ECDFs calculated for inclinometer BA04 at reference depths D01, D05, D10, D20, D30, and D40. A sample statistic-based approach was adopted, whereby a set of statistics were extracted from each velocity sample, namely: (a) the 0.05th sample quantile, (b) the 0.50th quantile or sample median, and (c) the 0.95th quantile. Hereinafter, these are denoted by $\xi_{IN,05}$, $\xi_{IN,md}$, and $\xi_{IN,95}$, respectively. While the median corresponds to a central probability level, the 0.05 and 0.95 quantiles represent the lower and upper bounds, respectively, of the 90% range of sample values. Characteristic sample values, defined here as

$$\xi_{ch} = \max\left[\mathrm{abs}\left(\xi_{IN,05}\right), \mathrm{abs}\left(\xi_{IN,95}\right)\right] \quad (1)$$
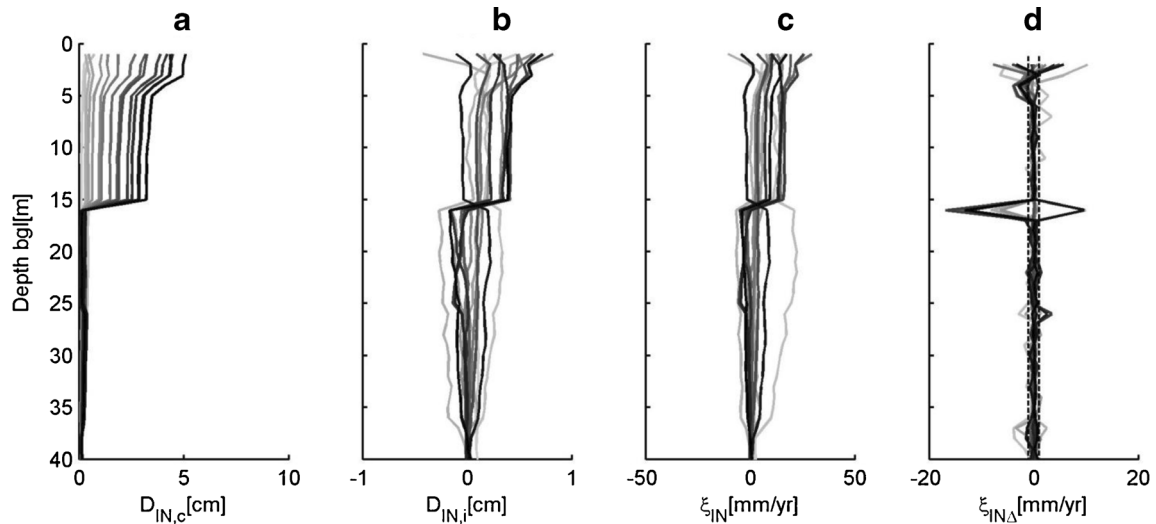
Fig. 4 Example of inclinometer data (inclinometer BA04): **a** cumulative displacement, **b** incremental displacement, **c** average velocity, and **d** differential average velocity. Data from more recent readings are shown in *darker lines*. *Dashed lines* in (**d**) delimit the range $\pm \xi_{IN\Delta t}$

were also retrieved from each sample. In the plots, darker lines correspond to shallower reference depths.

Figure 6 plots the median value of ξ_{IN} as estimated from inclinometer data at depth D01 for the inclinometers located inside or near the landslide perimeter. Similar plots were obtained for characteristic values, and for all reference depths. It was found that the vast majority of yearly velocities, even at very shallow depths, lie in the "extremely slow" range (i.e., less than 15 mm/year) according to the classification by Cruden and Varnes (1996). A general decrease with depth is observed for both sample median and sample characteristic values. Significant decreases in sample statistics are noted between D10 and D20 and between D30 and D40, suggesting that most movements occur between these two depths.

The spatial variability of inclinometer-measured displacement within the landslide perimeter was assessed through hierarchical clustering. The Euclidean distances (i.e., the differences in magnitude) between displacements measured by all pairs of inclinometers were calculated for each reference depth. Subsequently, hierarchical cluster trees were generated by applying the single linkage algorithm to each depth-specific pairwise Euclidean distance matrix. Dendrogram plots were then drawn for each reference depth. A dendrogram consists of U-shaped lines connecting objects (leaf nodes) in a hierarchical tree. The height of each U represents the difference in horizontal displacement between the two leaf nodes (i.e., inclinometers) being connected. Dendrogram plots of $\xi_{IN,md}$ are shown in Fig. 7, for reference depths D01 to D60.
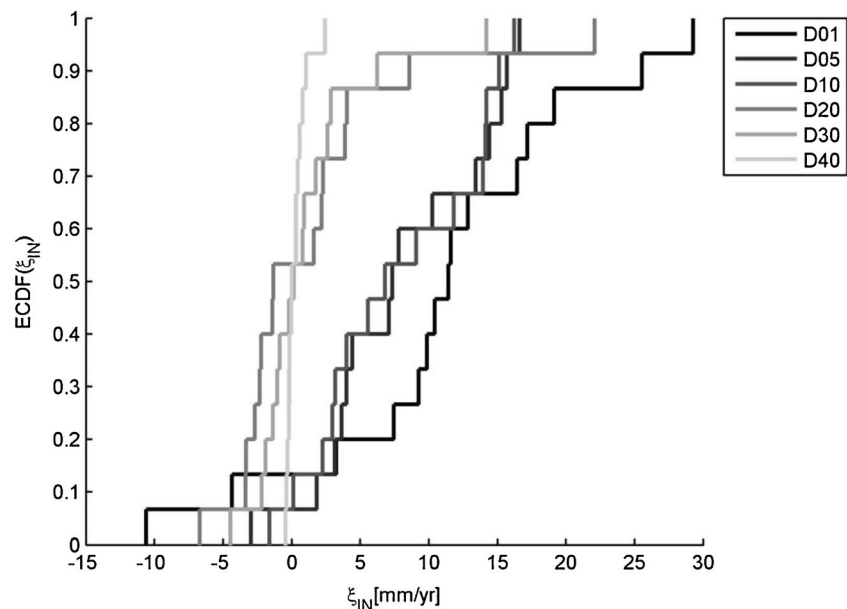
Fig. 5 Empirical cumulative distribution functions at reference depths D01 to D40 for inclinometer BA04
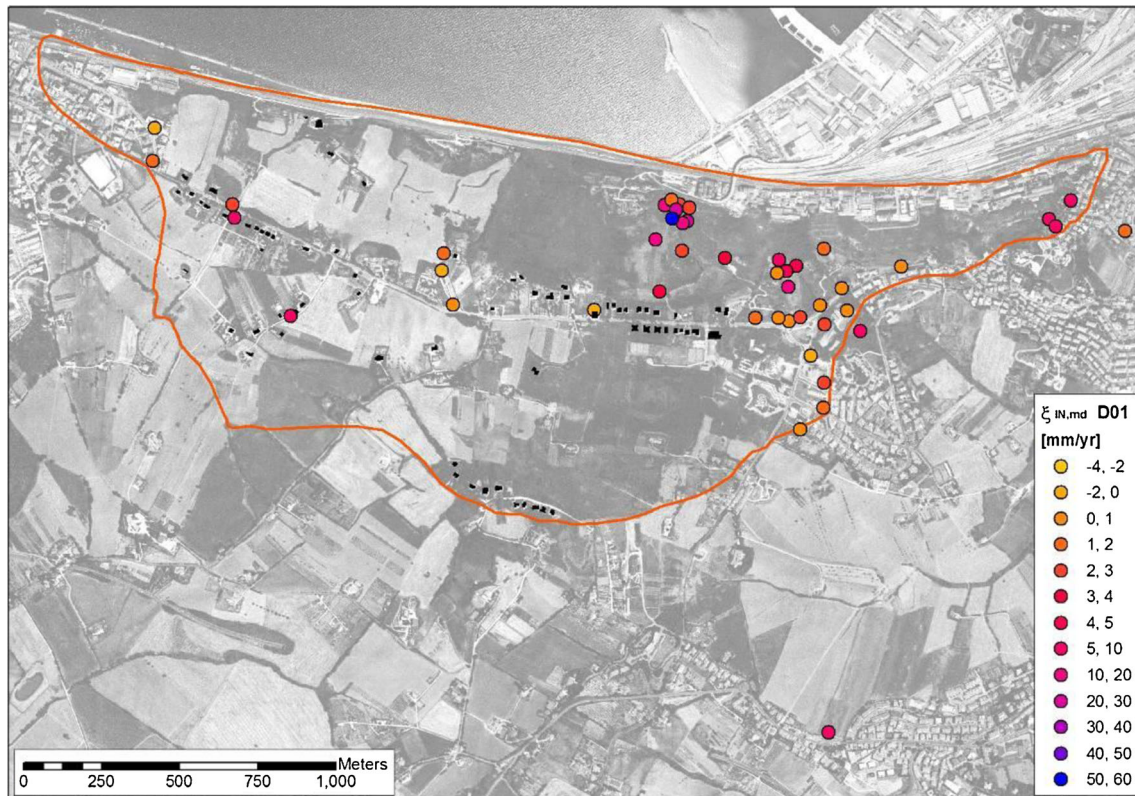
Fig. 6 Inclinometer-based estimates of $\xi_{IN,md}$ at reference depth D01

These plots allow the assessment of the depth-wise spatial distribution of horizontal displacement through georeferencing of the leaf nodes. The dendrogram analysis is useful in that it allows at least the qualitative a quantitative assessment of: (a) the degree of scatter in the magnitudes of horizontal velocity within the landslide area; (b) an insight into whether there are general spatial trends in horizontal velocity, i.e., if some areas display higher magnitudes of displacement than others. From a purely descriptive perspective, the parameterization of spatial variability from statistical dendrograms provides a reliable aid in the critical characterization of landslide kinematics. In the specific context of this case study and of the risk analysis presented in Uzielli et al. (2014), hierarchical clustering provides a useful tool in the selection of an appropriate technique for the spatialization of horizontal velocity as described in the following section. The main inference from the analysis of the dendrograms is the prevalence of slow movements throughout the landslide area, with only localized larger velocities in the Barducci area.

Spatial interpolation of inclinometer data

As detailed in Uzielli et al. (2014), ground displacement is taken as the reference parameter for the characterization of landslide intensity for the purpose of risk estimation for buildings. In order to estimate hazard as a displacement-dependent parameter, it is necessary to estimate ground displacement at the locations of the buildings themselves. As these locations are not coincident with those of the inclinometers, it may be convenient to spatialize the average yearly velocity (subsequently used in the calculation of displacement) from the available point estimates using interpolation algorithms. Geostatistical interpolation algorithms are suitable for this purpose. Radial basis functions (RBF) with regularized splines were thus implemented to spatialize ξ_{IN} values beyond the discrete set of monitoring locations to areal locations relevant for risk estimation to the set of 39 buildings. RBFs are exact deterministic interpolators providing prediction surfaces that are comparable to the exact form of geostatistical kriging while not requiring formal investigation of spatial autocorrelation, nor parametric statistical assumptions about the data. Moreover, from the statistical dendrogram analysis presented in the previous section, it appears that no general spatial trends in ξ_{IN} are present. RBF, which does not require the explicit preliminary selection of a functional form for a spatial trend, is thus a suitable option. It is intuitive that, due to the nonuniform spatial distribution of inclinometer locations and to the significant distances between clusters of inclinometers, the results of geostatistical interpolation are not of uniform quality in terms of reliability, with estimates pertaining to spatial locations which are more distant from sampled locations being less reliable.

The spatialization of displacements must duly account for—and be consistent with—available knowledge and information regarding the tectonic and geomorphological features of the landslide area described in "Geological, tectonic, geotechnical, and hydrological setting." A set of seven subzones were identified based on the observed and/or inferred existence of macro-discontinuities as shown in Fig. 3. Continuity in the displacement field can be envisaged within each sub-zone, but it is less likely to exist across subzones.

The external contour of the union of the subzones was taken by considering at most a 150-m outer offset from the inclinometers as
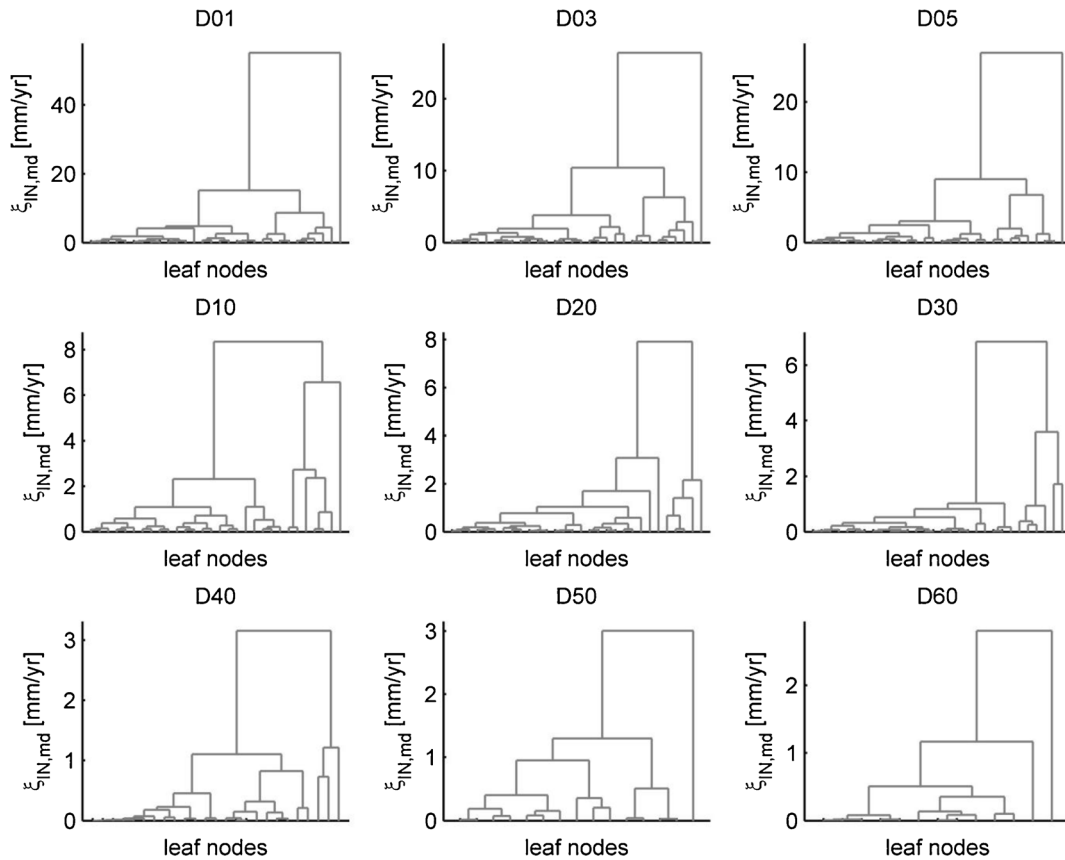
Fig. 7 Hierarchical dendrograms of $\xi_{IN,md}$ for reference depths D01 to D60

to increase the presumed reliability of geostatistical estimates. A total of 39 buildings fall into subzones I, II, and III. Risk estimation is conducted for these buildings in Uzielli et al. (2014). Subzones IV, V, VI, and VII are included solely for the purpose of characterizing landslide kinematics.

Figure 8 plots the RBF interpolations of median ξ_{IN} inside the seven subzones at reference depth D01. Similar plots (not shown here) were generated for the other reference depths. Most median velocity values fall within the "extremely slow" category in the landslide velocity scale, for which construction is "possible with precautions" according to Cruden and Varnes (1996). Characteristic values fall mostly within the "very slow" category, indicating that the majority of permanent structures are likely to suffer damage as a consequence of sliding. The highest velocity values are localized in a small portion of sub-zone VII in the Barducci area.

Characterization of vertical sliding velocity by radar interferometry
In the present study, radar interferometer data are used to estimate the vertical component of surficial sliding velocity. Such component will be used jointly with the horizontal component obtained from inclinometer data for the quantification of hazard as detailed in Uzielli et al. (2014). Multi-interferograms Satellite SAR Interferometry (PSI) technique is based on the use of long series (the larger the number of images the more precise and robust the results) of coregistered, multi-temporal SAR imagery. Rapid advances in both remote sensing sensors and data processing algorithms allowed achieving significant results in recent years,

underscored by numerous applications. The application of PSI techniques to the study of slow-moving landslides (i.e., with velocity<13 mm/month according to Cruden and Varnes (1996) is a relatively new and challenging topic (see, e.g., Cascini et al. 2010; Lu et al. 2012; Righini et al. 2012; Cigna et al. 2012; Tofani et al. 2013a).

Among the various PSI techniques, the PSInSAR™ (Ferretti et al. 2001; Colesanti et al. 2003) was used in this study. The PSInSAR™ has shown its capability to provide information about ground deformations over wide areas, making this approach suitable for both regional and slope scale mass movements investigations. Through a statistical analysis of the signals backscattered from a network of individual, phase coherent targets, this approach retrieves estimates of the displacements occurred between different acquisitions, by distinguishing the phase shift related to ground motions from phase component due to atmosphere, topography, and noise.

PSI targets (permanent scatterers (PS)) are stable radar benchmarks on the ground surface that are often represented by manmade structures. The accuracy in the definition of ground displacements is theoretically dependent on the radar wavelength which is used, being the PSI technique basically a phase difference computation. This would mean millimetric accuracy using SAR images from ERS, ENVISAT and RADARSAT satellites, for example.

The acquisition of the SAR satellite occurs along two different polar orbits, descending from north to south and ascending from south to north. Displacements are measured along a unit vector
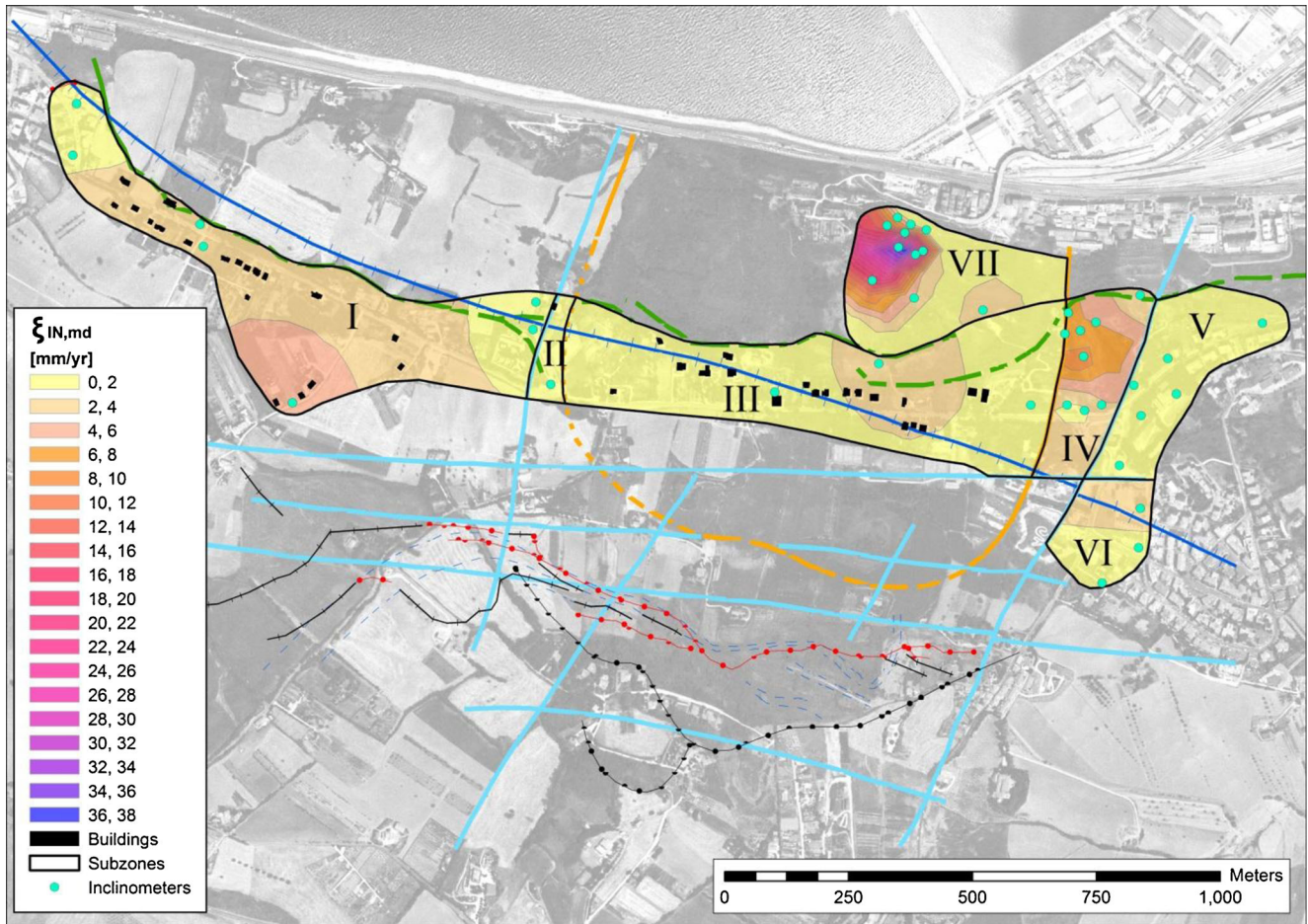
Fig. 8 RBF interpolation of $\xi_{IN,md}$ at D01 from inclinometer data

codirectional to the satellite defined as line-of-sight (LOS). Being the orbit of SAR satellites polar, it is impossible to estimate the component of displacement along the N–S direction on the azimuth plane. The vertical displacement is given, with reference to Fig. 9, by

$$D_{VT} = \frac{D_{asc}\sin\theta_{des} - D_{des}\sin\theta_{asc}}{\sin\theta_{des}\cos\theta_{asc} - \sin\theta_{asc}\cos\theta_{des}} \qquad (2)$$

in which D_{asc} and D_{des} are the measured ascending and descending displacements, respectively, and θ_{asc} and θ_{des} are the incidence angles of the ascending and descending satellite orbits, respectively. For further information on the PSI technique and its applications to landslide studies, the reader is referred to Ferretti et al. (2001), Colesanti et al. (2003), Farina et al. (2006), Colesanti and Wasowski (2006), Cigna et al. (2012), and Tofani et al. (2013b).

Statistical estimation of vertical displacements

For the Ancona site, PSInSAR data from satellites ERS-1 and ERS-2 of the European Space Agency (ESA) were available for 42 ascending images (from 1992-08-23 to 2000-12-13) and 66 descending images (from 11 Jun 1992 to 10 Dec 2000); data from ENVISAT (ENV) were available for 36 ascending images (from 26 Feb 2003 to 22 Oct 2008) and 28 descending images (from 15 Dec 2002 to 23 Nov 2008).

For both ERS and ENV, the incidence angles were $\theta_{asc} = -23°$ (ascending) and $\theta_{des} = +23°$ (descending), respectively. Positive values of D_{VT} indicate uplifts while negative values indicate settlements. These conventions are also valid for calculated velocities. The area of analysis was restricted to the 500-m-wide buffer offsetting the landslide perimeter. A total of 6,406 (3,811 ascending; 2,595 descending) and 6,575 (2,638 ascending; 3,937 descending) PS were available for ERS and ENV, respectively. The PS located inside or near the landslide perimeter are shown in Fig. 3.

As PS pertaining to the ascending orbit generally do not correspond to those pertaining to the descending orbit, it is necessary to establish a criterion for merging D_{asc} and D_{des} measurements from distinct PS, and for geo-referencing the resulting values of D_{VT}. If ascending and descending measurements pertain to spatial locations, which are geographically distant, or to readings, which are chronologically too distant, results are not likely to be correct or meaningful.

Couples of conjugate PS were identified on the basis of a Euclidean distance criterion, the latter being calculated from the available N and E coordinates of the ascending and descending Permanent Scatterers. A maximum projected plan distance threshold of 10 m was established. Pseudo-locations were calculated as geographic midpoints of the segment connecting the conjugate ascending and descending PS. In a temporal perspective, the maximum acceptable lag between ascending and descending
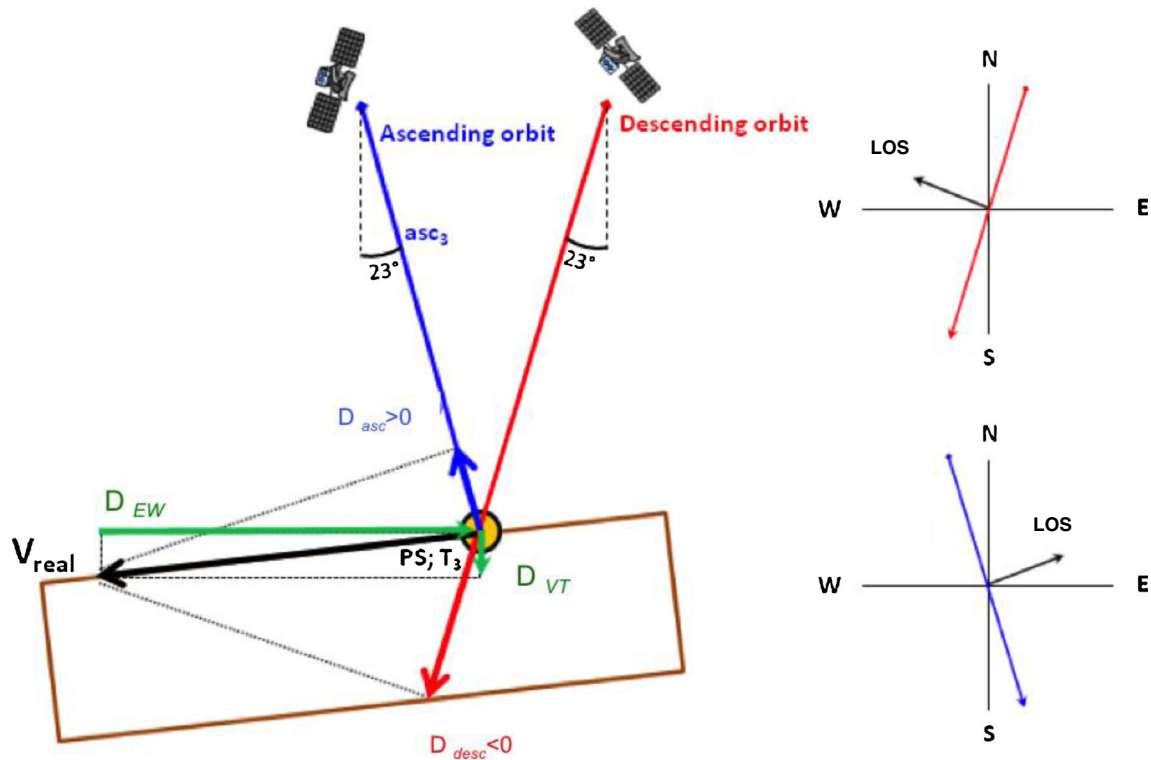
Fig. 9 Extraction of vertical and horizontal (E–W) deformation components, projecting the ascending and descending acquisition geometries (modified from Tofani et al. 2013b)

measurement dates was set at 50 days. Pseudo-dates were calculated as average dates between the conjugate dates of ascending and descending measurements. By the above criteria, a total of 1,318 and 1,182 pseudo-locations were generated for ERS and ENV, respectively. The associated number of pseudo-dates (and calculated vertical velocities) was 131 for ERS and 58 for ENV. Figure 10 illustrates an example calculation of vertical displacements from the ENV dataset. Subplot (a) shows the chronological sequences of ascending and descending measurements D_{asc} and D_{des} taken in distinct dates for the pair of conjugate PS "A1RAE" (ascending) and "A08PY" (descending); subplot (b) plots the resulting vertical displacements at the pseudo-location ENV-PO120. It should be noted that: (a) pseudo-dates generally do not coincide with effective reading dates; and (b) one ascending measurement can be associated with more than one descending measurement (or vice versa), as long as the temporal lag does not exceed the present threshold. Thus, the larger number of pseudo-dates in comparison with the effective dates of ascending and descending readings.

Average daily vertical velocities between consecutive pseudo-dates were calculated by dividing the differential displacements by the time interval between pseudo-dates. Following the assessment of temporal stationarity of calculated velocities by Kendall's tau test as detailed for inclinometer data, vertical velocity was expressed on a yearly basis by multiplication by 365. The latter parameter, indicated by ξ_{VT} was thus taken as reference parameter for the characterization of the vertical component of sliding. Figure 11 illustrates an example output chrono-plot of ξ_{VT} at pseudo-location ENV-P0120.

ECDFs were calculated for samples of ξ_{VT} from the ERS and ENV data sets at each pseudo-location. An example ECDF is shown in Fig. 12 for pseudo-location ENV-P0120. Sample median

and characteristic values as defined by Eq. (1) were retrieved for ξ_{VT} for both ERS and ENV pseudo-locations.

Comparison of ERS and ENV data
Figure 13a, b plots, respectively and comparatively, the relative frequency histograms of median and characteristic values of ξ_{VT} calculated from ERS and ENV data for the complete set of pseudo-locations. The significant differences in ξ_{VT} between the samples of ERS and ENV data suggest a closer investigation into the relevance of the data for the assessment of current slope kinematics. ERS data were acquired in the period 1992–2000, i.e., before the remediation and consolidation works, whereas ENV data refer to the post-remediation period (2002–2008). Cotecchia (2006) attributed the decrease in the magnitudes of monitoring displacement readings from 2001 to present to the activation of the drainage system which was constructed between 1999 and 2000 and which, according to the same Author, significantly increased slope stability, lowering the piezometric level inside the landslide area by "up to some 10 m" and reducing both shallow and deep-seated sliding phenomena.

Figure 13 shows that median values of ξ_{VT} are fairly coincident (relative frequency histograms are approximately superimposed). However, characteristic values of ERS data display considerably larger values than ENV data, indicating the occurrence of more significant sliding in the ERS measurement period. This observation could be related to the effects of the remediation works. In other words, the implementation of slope stabilization measures possibly resulted in an effective mitigation of larger movements in the slope.

In the present study, as detailed in Uzielli et al. (2014), hazard estimation relies on the probabilistic simulation of average vertical yearly velocity from sampling distributions defined from output
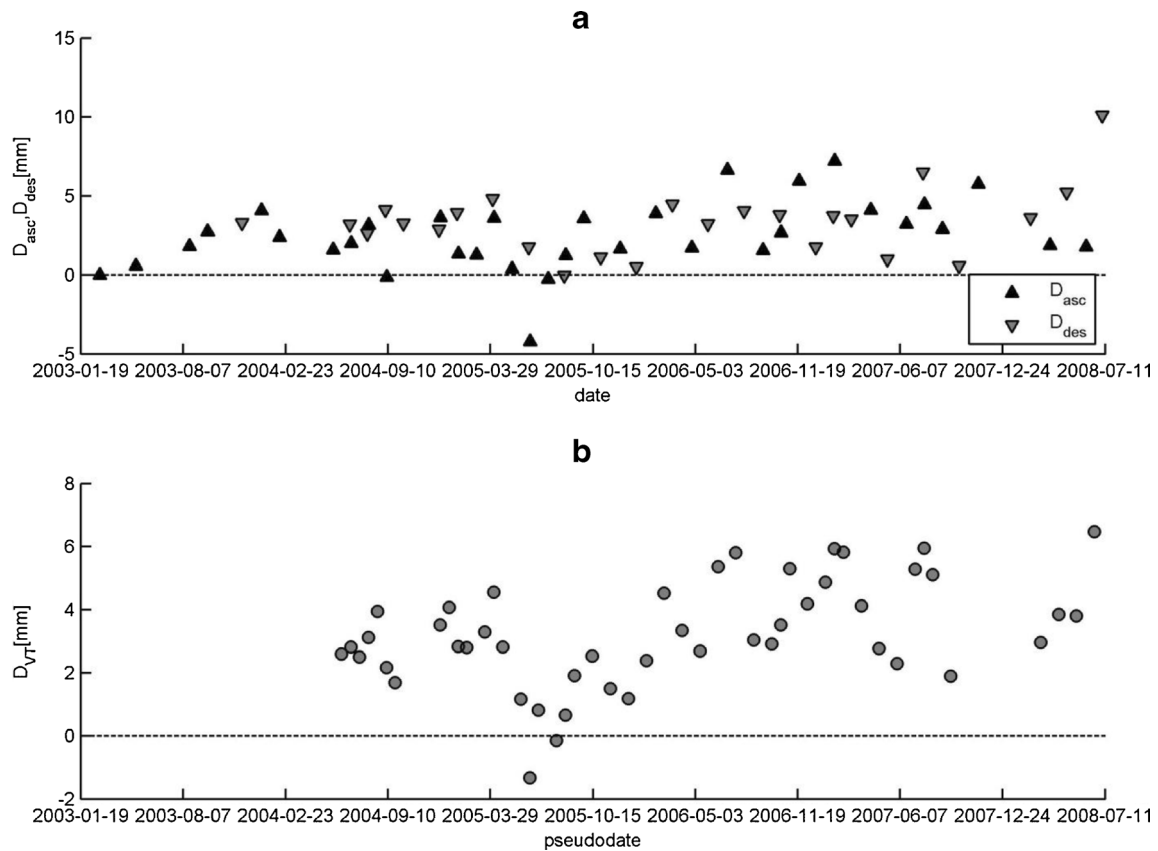
Fig. 10 **a** SAR interferometer data from conjugate permanent scatterers and **b** example calculation of vertical displacements at pseudo-location ENV-P0020

relative frequency histograms of median vertical velocity. Though sample median values from ERS and ENV data sets are almost coincident, extreme (lower and upper) sample quantiles of ERS data differ considerably from corresponding ENV quantiles. Thus, ERS data, which refers to a prestabilization period, should not be examined jointly with ENV data. Only the latter are considered and processed for the purpose of risk estimation as detailed in Uzielli et al. (2014).

Spatialization of PS data

The scarcity of PS inside the subzones is evident in Fig. 3. There are five spatially well-distributed PS in subzone I; subzone III includes

four PS which, however, are essentially superimposed. Subzone V includes two targets, whereas all other subzones are empty. This suggests that the use of geostatistical interpolation may overall not be advocated to spatialize the vertical component of sliding velocity. Spatialization was thus performed subjectively by examining median and characteristic values of ξ_{VT} calculated as described in "Statistical estimation of vertical displacements." Figure 14 plots the subjectively spatialized median values of ξ_{VT} for ENV data. Spatialization of vertical velocity from PS data are necessary for the probabilistic estimation of hazard as described in Uzielli et al. (2014).
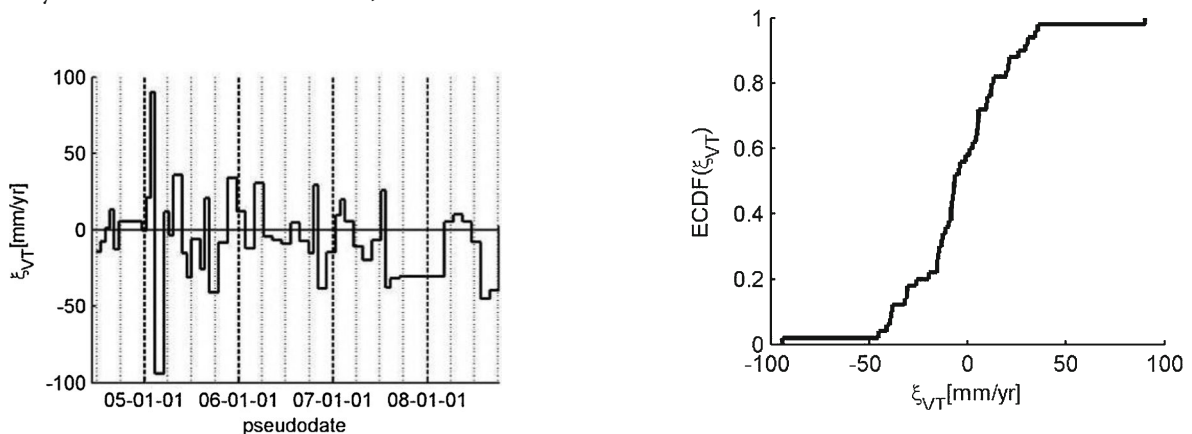
Fig. 11 Chrono-plot of ξ_{VT} at pseudo-location ENV-P0120

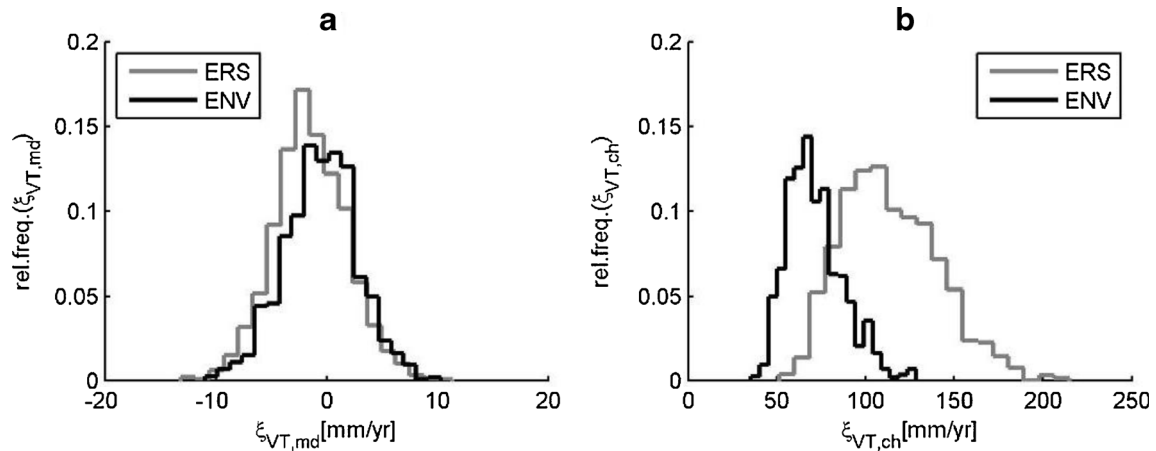**Fig. 12** Empirical cumulative distribution function of ξ_{VT} for pseudo-location ENV-P0120

Fig. 13 Relative frequency histograms of median and characteristic sample values of ξ_{VT}: comparison between ERS and ENVISAT data

Concluding remarks

Inclinometer and PS data were processed statistically to obtain estimates of horizontal and vertical sliding velocities, respectively, specifically for the purpose of the quantitative risk estimation detailed in Uzielli et al. (2014). The two velocity components were estimated separately using statistical methods calibrated, in terms of complexity and scope, to the quantity and quality of available data. Both sets of measurements clearly and consistently show that slope deformation processes are still active, thus inherently justifying the risk estimation effort. The magnitudes of horizontal and vertical velocity are comparable, and range (in median values) between "extremely slow" and "very slow" in the landslide velocity scale. Characteristic values also fall in the "very slow" category, confirming that the Ancona landslide is a markedly slow-moving
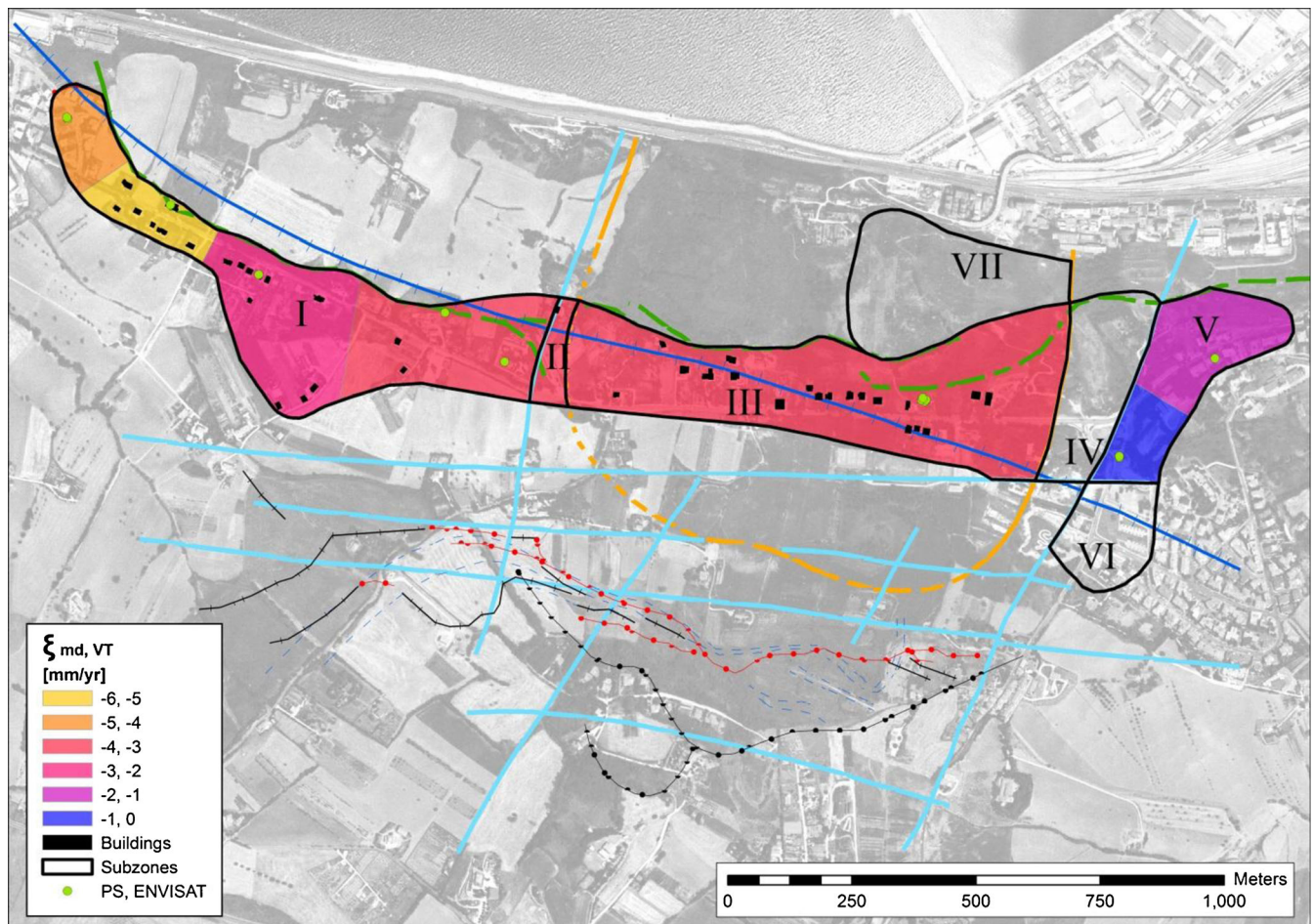

Fig. 14 Spatialized vertical velocity $\xi_{VT,md}$ for ENVISAT data

landslide which, however, anticipating the risk estimation outputs given in Uzielli et al. (2014), poses a threat to existing structures.

A detailed inference of landslide kinematics appears to be inherently problematic due to the inherent imprecision, inaccuracy and uncertainty associated with the interpolation procedure (due to the quantity and quality of available data and to the nonuniform spatial distribution of data sources). Nonetheless, examination of the spatial distribution of horizontal and vertical sliding velocity suggests that these are compatible—and consistent with the kinematic and typological features of the landslide suggested by other Authors and described in "Typological description." Thus, the results obtained herein are deemed acceptable for further processing in the risk analysis effort as described in Uzielli et al. (2014).

The limitations in the quantity and quality of data have led to several simplifications. First, the lack of reliable azimuth measurements did not allow a detailed modeling of the direction of velocity. While this fallacy would result in a relevant limitation in the context of a descriptive analysis of the landslide model, it does not substantially hinder the use of estimated velocities for risk estimation purposes, since it is plausible to suppose that the damage potential to the buildings is sensitive to the magnitude of velocity (and, thus, displacement) but is invariant to the direction of sliding. Second, the impossibility to obtain readings in the North–South direction, which is known to be the principal direction of sliding given the orientation of the slope, essentially impedes the analysis of horizontal velocity from PSInSAR measurements. These are, however, useful for the characterization of the vertical component of sliding. Third, the quantitative results obtained herein are based solely on available monitoring data collected between 2002 and 2008, i.e., in absence of exceptional events. As discussed in "Estimation of horizontal sliding velocity," this entails that the statistical modeling of landslide kinematics does not extend to exceptional scenarios such as the 1982 landslide. However, the operational framework developed in the paper can accept additional data and accommodate any scenario. In the context of risk analysis, this entails that the risk estimated from the monitored displacement refers to a "normal" situation and should thus be seen as a lower-bound estimate. Anticipating the results of the risk analysis detailed in Uzielli et al. (2014), this lower-bound estimate emphasizes the fact that, however slow, the Ancona landslide is expected to induce significant damage in buildings located inside its perimeter in the medium-long term even in absence of extreme events. Moreover, the risk estimation procedure proposed in Uzielli et al. (2014) extends to exceptional scenarios through the definition and calibration of an analytical function parameterizing landslide intensity (i.e., destructive potential) for displacement levels such as those observed during the 1982 event.

Despite the aforementioned limitations which are inherent to the application of statistical techniques to a real and complex case study, the results of the statistical estimation of sliding velocity are deemed adequate in terms of consistency with existing experience regarding the Ancona landslide and worthy of practical implementation in the quantitative risk estimation detailed in Uzielli et al. (2014).

References

Bally AW, Burbi L, Cooper C, Ghelardoni R (1988) Balanced sections and seismic reflections profiles across the Central Apennines. Mem Soc Geol Ital 35:257–310

Bracci V (1773) Relazione alla visita fatta per ordine della Congregazione de B. Governo nei mesi di aprile e maggio 1773 a un tratto di strada Flaminia. Archivio di Stato, sez. IV, Ancona

Cardellini S, Osimani P (2008) Living with landslide: the Ancona case history and early warning system. Proc. First World Landslide Forum, Tokyo, pp 473–476

Cascini L, Fornaro G, Peduto D (2010) Advanced low- and full resolution DInSAR map generation for slow-moving landslide analysis at different scales. Eng Geol 112:29–42

Cassinis R, Tabacco I, Bruzzi GF, Corno C, Brandolini A, Carabelli E (1985) The contribution of geophysical methods to the study of the great Ancona landslide (December 13, 1982). Geoexploration 23:363–386

Cigna F, Bianchini S, Casagli N (2012) How to assess landslide activity and intensity with Persistent Scatterer Interferometry (PSI): the PSI-based matrix approach. Landslides 5:1–17

Colesanti C, Wasowski J (2006) Investigating landslides with space-borne Synthetic Aperture Radar (SAR) interferometry. Eng Geol 88:173–199

Colesanti C, Ferretti A, Prati C, Rocca F (2003) Monitoring landslides and tectonic motions with the Permanent Scatterers Technique. Eng Geol 68:3–14

Colombo P, Esu F, Jamiolkowski M, Tazioli GS (1987) Studio sulle opere di stabilizzazione della frana di Posatora e Borghetto. ITALGEO. Report for the Ancona Town Council (Unpublished)

Coltorti M, Dramis F, Gentili B, Pambianchi G, Crescenti U, Sorriso-Valvo M (1985) The december 1982 Ancona landslide: a case of deep-seated gravitational slope deformation evolving at unsteady rate. Z Geomorphol 29(3):335–345

Coltorti M, Dramis F, Gentili B, Pambianchi G, Sorriso-Valvo M (1986) Aspetti geomorfologici della frana di Ancona. In: "La grande frana di Ancona del 13 Dicembre 1982". Studi Geologici Camerti, Numero Speciale: 29–40

Cotecchia V (1994) Interventi di consolidamento del versante settentrionale del Montagnolo e della relativa fascia costiera interessati dai movimenti di massa del 13 Dicembre 1982—Studi e progetto di massima. Report for the Ancona Town Council (Unpublished)

Cotecchia V (2000) Interventi di consolidamento del versante settentrionale del Montagnolo e della relative fascia costiera interessati dai movimenti di massa del 13 Dicembre 1982. Approfondimenti tecnico-scientifici eseguiti per le opere di rinterro previste nel progetto di massima. Report for the Ancona Town Council (Unpublished)

Cotecchia V (2001) Consulenza tecnica per il coordinamento degli studi e delle operazioni di controllo relative all'area della grande frana di Ancona-Relazione. Report for the Ancona Town Council (Unpublished)

Cotecchia V (2006) Experience drawn from the great Ancona landslide of 1982. The Second Hans Cloos Lecture. Bull Eng Geol Environ 65(1–41):2006. doi:10.1007/s10064-005-0024-z

Cotecchia V, Simeone V (1996) Studio dell'incidenza degli eventi di pioggia sulla grande frana di Ancona del 13.12.1982. Proc. Int. Conf. "Prevention of hydrogeological hazards: the role of scientific research", 19–29

Cotecchia V, Grassi D, Merenda L (1995) Fragilità dell'area urbana occidentale di Ancona dovuta a movimenti di massa profondi e superficiali ripetutesi nel 1982. Atti del I Convegno del Gruppo Nazionale di Geologia Applicata & Idrogeologia 30(1):633–657

Crescenti U (1986) Notizie Precedenti. In: "La grande frana di Ancona del 13 Dicembre 1982". Studi Geologici Camerti, Numero Speciale: 13–23

Crescenti U, Nanni T, Rampoldi R, Stucchi M (1977) Ancona: considerazioni sismotettoniche. Boll Geofis Teor Appl 73(74):33–48

Crescenti U, Ciancetti GF, Coltorti M, Dramis F, Gentili B, Melidoro G, Nanni T, Pambianchi G, Rainone Semenza E, Sorriso-Valvo M, Tazioli GS, Vivalda P (1983) La grande frana di Ancona del 1982. Collana "Problemi del territorio". Spoleto 4–7 maggio 1983

Crescenti U, Curzi PV, Gallignani P, Gasperini M, Rainone M, Stefanon A (1984) La frana di Ancona del 13 dicembre 1982: Indagini a mare. Memorie della Società Geologica Italiana 27:545–553

Crescenti U, Calista M, Mangifesta M, Sciarra N (2005) The Ancona landslide of December 1982. Gior Geol Appl 1:53–62

Cruden DM, Varnes DJ (1996) Landslide types and processes. Landslide investigation and mitigation, TRB Special Report 247, National Academy Press, Washington, DC: 36–75

Cunietti M, Bondi G, Fangi G, Moriondo A, Mussio L, Proietti F, Radicioni F, Vanossi A (1986) Misure topografiche ed aerofotogrammetriche. In: La grande frana di Ancona del 13 Dicembre 1982. Studi Geologici Camerti, Numero Speciale: 41–82

Curzi PV, Stefanon A (1986) Indagini a mare. In: La grande frana di Ancona del 13 Dicembre 1982. Studi Geologici Camerti, Numero Speciale: 135–144

De Bosis F (1859) Il Montagnolo: studi ed osservazioni. Encicl Contemp, Gabrielli, Fano

Dramis F, Farabollini P, Gentili B, Pambianchi G (2002) Neotectonics and large-scale gravitational phenomena in the Umbria-Marche Apennines, Italy. In: Seismically induced ground ruptures and large Scake mass movements. Field Excursion and Meeting 21–27 September 2001. APAT, Atti 4/2002: 17–30

Farina P, Colombo D, Fumagalli A, Marks F, Moretti S (2006) Permanent Scatterers for landslide investigations: outcomes from the ESA-SLAM project. Engineering Geology 88:200–217

Ferretti A, Prati C, Rocca F (2001) Permanent scatterers in SAR interferometry. IEEE Trans Geosci Remote Sensing 39(1):8–20

Lu P, Casagli N, Catani F, Tofani V (2012) Persistent scatterers interferometry hotspot and cluster analysis (PSI-HCA) for detection of extremely slow-moving landslides. Int J Remote Sens 33:466–489

Michetti AM, Brunamonte F (2002) Some remarks on the relations between the 1972 Ancona earthquake sequence and the Ancona landslide. In: Comerci V., ed., Seismically induced ground ruptures and large scale mass movements APAT—INQUA Sub-commission on "Paleoseismology", Working Group on "Mountain Building", Field Excursion and Meeting, 21-27 September, 2001, Field Trip Guide Book. Atti APAT, 4/2002: 31–34

Righini G, Pancioli V, Casagli N (2012) Updating landslide inventory maps using persistent scatterer interferometry (PSI). Int J Remote Sens 33(7):2068–2096

Santaloia F, Cotecchia V, Monterisi L (2004) Geological evolution and landslide mechanisms along the central Adriatic coastal slopes. Proc Skempton Conf 2:943–954

Segré C (1920) Criteri geognostici per il consolidamento della falda franosa del Montagnolo, litorale Ancona-Falconara. Boll Soc Geol Ital 38:99–131

Stucchi E, Mazzotti A (2009) 2D seismic exploration of the Ancona landslide (Adriatic Coast, Italy). Geophysics 74–5:B139–B151

Tofani V, Segoni S, Agostini A, Catani F, Casagli N (2013a) Technical note: use of remote sensing for landslide studies in Europe. Nat Hazards Earth Syst Sci 13:1–12. doi:10.5194/nhess-13-1-2013

Tofani V, Raspini F, Catani F, Casagli N (2013b) Persistent scatterer interferometry (PSI) technique for landslide characterization and monitoring. Remote Sens 5:1045–1065

Uzielli M, Catani F, Tofani V, Casagli N (2014) Risk analysis for the Ancona landslide—II: estimation of risk to buildings. Submitted as companion paper

M. Uzielli (✉)
Georisk Engineering S.r.l.,
Florence, Italy
e-mail: muz@georisk.eu

F. Catani · V. Tofani · N. Casagli
Department of Earth Sciences,
University of Florence,
Florence, Italy